

# Analysis, results and assessment of the NICMOS warm-up monitoring program

---

T. Böker, J. Bacinski, E. Bergeron, D. Gilmore, S. Holfeltz, B. Monroe, M. Sosey  
April 21, 1999

---

## ABSTRACT

*We summarize the results of the NICMOS warmup monitoring program. Instrument parameters such as quantum efficiency, dark current, focus behavior, bias offsets, and saturation levels have been measured and are projected onto the expected temperature range for operation with the NICMOS Cooling System (NCS). We estimate NICMOS performance during the NCS era, and briefly discuss possible implications for the cycle 9 calibration program.*

---

## 1. Introduction

Shortly after its on-orbit installation, it was discovered that the NICMOS dewar suffered from a thermal anomaly that led to a higher than expected sublimation rate of the solid nitrogen coolant, and thus a shortened lifetime. Thermal modeling - performed during spring of 1998 by Ball Aerospace - estimated the nitrogen to be exhausted by the end of Dec. 1998, with an uncertainty of around 30 days. The main NICMOS science program was thus completed on Nov. 15, 1998, and the warm-up monitoring program was activated. The main goal of this program was to estimate NICMOS scientific performance at the higher operating temperatures ( $\sim 77$  K compared to  $\sim 62$  K over most of the NICMOS life) that are expected after the installation of the NICMOS Cooling System (NCS).

The monitoring program had three elements:

- Proposal 7961 (pure parallel) took lamp flats four times a day in a number of filters in all three cameras. The goal was to follow the QE variations as a function of temperature and wavelength to provide sensitivity estimates under NCS.
- Prop. 7962 (pointed) observed a star cluster twice a week in order to monitor possible focus variations due to varying mechanical stresses in the dewar.

- Prop. 7963 (internal) took darks in all three cameras once every orbit unused by the other two monitoring proposals. This proposal was designed to allow monitoring of both the dark current of the detectors and possible temperature-induced electronic effects, such as bias drifts. Prop. 7963 was extended by Prop. 8093, since the warmup occurred later than anticipated, i.e. after the last scheduled observation of Prop. 7963. Table 1 lists the details of the program.

**Table 1.** Components of the warm-up program

Prop. #	Target	Purpose	Filter	Sequence	NSAMP
7961	Random	Flatfields to derive DQE	NIC1: F110W, F160W NIC2: F110W, F160W NIC3: F110W, F160W, F222M	Step8, Step16 Step1, Step8 Step1, Step1, Step1	9, 10 10, 8 6, 10, 10
7962	NGC 3603	Focus	NIC2: F110W NIC3: F108N	MCAMRR STEP8	4 9
7963 (8093)	blank	Dark current	blank	STEP64	25

Except for a brief NICMOS suspend on Dec. 24 for reasons unrelated to the warm-up, all programs executed nominally, and the data were made accessible to the NICMOS group immediately. This allowed a near real-time monitoring of instrumental performance, which was augmented by continuous sampling of telemetry temperature readings. The following sections describe the results of the data analysis.

## 2. Warm-up Profile

### *Model predictions*

The thermal modeling of the NICMOS dewar performed by Ball had the goal to estimate the date of cryogen depletion and to identify signatures in the temperature profiles that could be used as early warning signs that warm-up is imminent. The model was designed to match the observed depletion rates and temperature data up to March 1998 and resulted in a number of predictions for the actual warm-up:

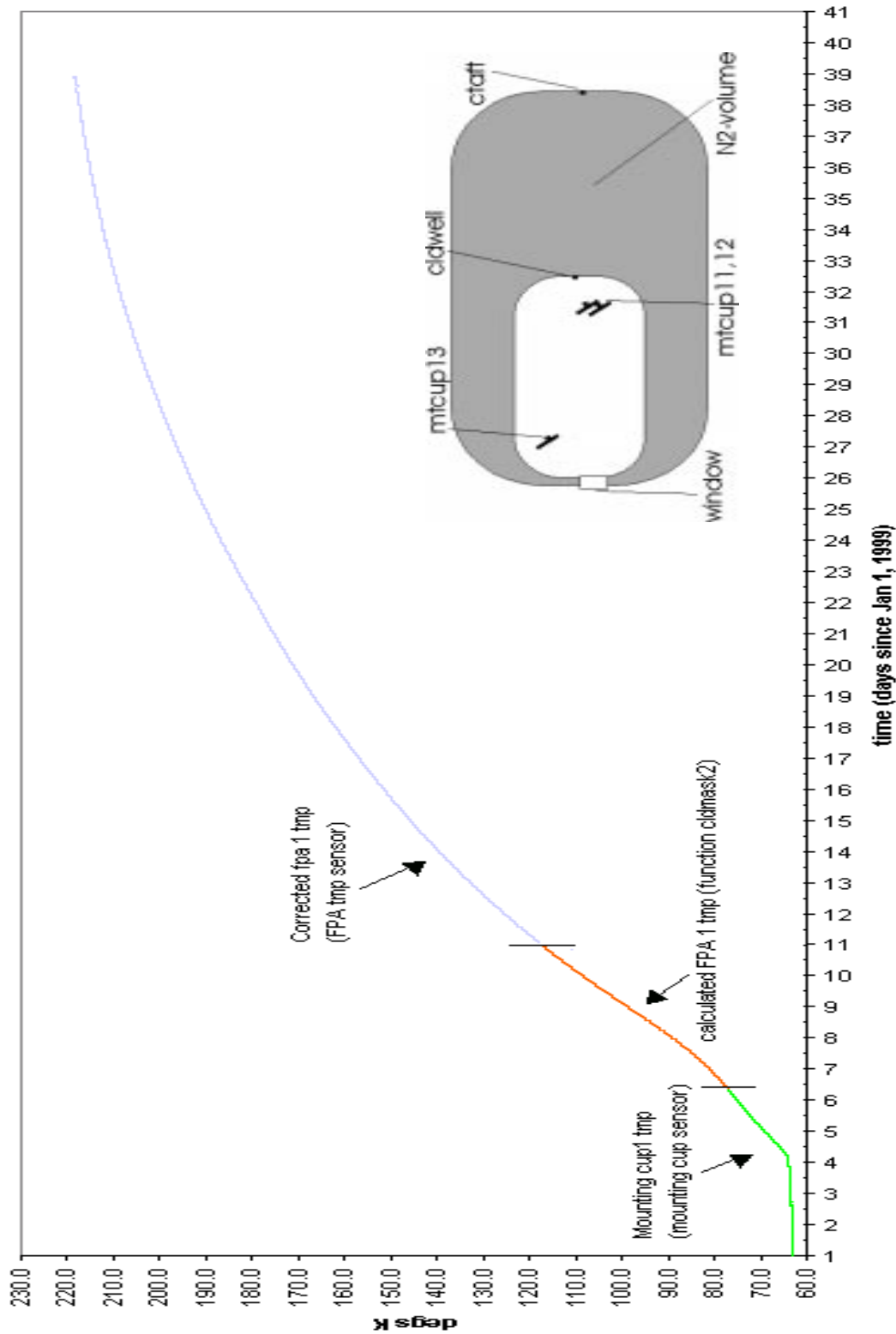
1. Depletion occurs late Dec. 1998.
2. About 30-40 days before depletion, the temperature difference between the detector mounting cups and the aft end of the dewar will decrease, because the nitrogen ice will detach from the aft end wall at that time.
3. After depletion, the mounting cup temperatures will increase at a rate of 4.5 K/day, based on a constant thermal short strength of 10.2 mW/K.

In addition to the thermal modeling, a mechanical analysis based on a finite element model of the NICMOS dewar was performed by Mega Engineering, with the goal to estimate any stresses that might occur during warm-up. Special emphasis was put on the question of whether or not the thermal short could be broken by either leaving the Thermo-Electric Coolers (TECs) on or switching them off after cryogen depletion. The result of this study was that the short should persist and even slightly increase in either scenario, slightly more so when leaving the TECs on. However, in neither scenario should the mechanical stresses exceed those experienced after the NICMOS installation. It was therefore decided to leave the TECs on during the warm-up and throughout the warm period until SM3 in order to avoid the risk of failure.

### ***Measurements***

On Jan. 4th, 1999, the mounting cup temperatures - and all other dewar temperatures - started to rise sharply, indicating that ice depletion was reached. Figure 1 shows the location of some temperature sensors inside the NICMOS dewar, as well as the temperature profile of the camera 1 detector. The use of the mounting cup sensors is limited to temperatures below 78.1 K by the dynamic range of their A/D converters. No temperature data are available from the time these sensors saturated on Jan. 6 until the focal plane array (FPA) sensors were activated on Jan. 11, after NICMOS data taking was suspended. The FPA sensors are mounted directly on the three NICMOS chips and are not used during normal operations because they produce both thermal emission and bias variations.

**Figure 1:** Temperature profile of camera 1. The inlay shows the location of some temperature sensors inside the dewar. The FPA sensors are located directly on the detector chips.



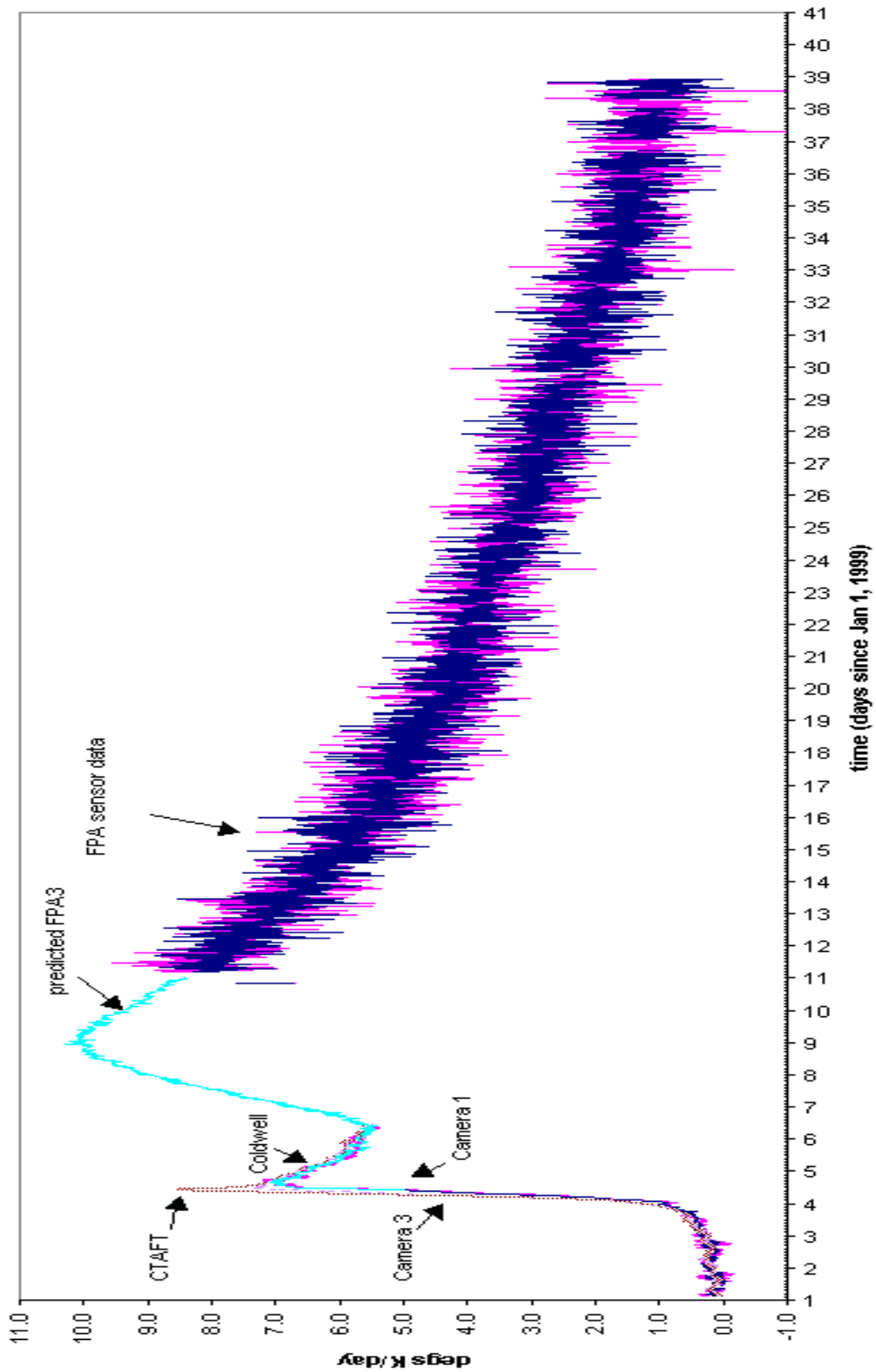
It quickly became clear that the warm-up rate was significantly higher than predicted by the models. Fig. 2 shows the (2.5 h averaged) warm-up rates of cameras 1 and 3, as determined from the measurements shown in Fig. 1, in comparison to the cold well (coldwell) and the aft end of the dewar (ctaft). The rates of all sensors show a basically identical behavior, namely a steep increase to  $\sim 7$  K/day on Jan, 4, followed by an exponential decline to  $\sim 5.5$  K/day on Jan. 7.<sup>1</sup> The dewar aft end showed the highest peak rate, since at that time it was the coldest point of the dewar. After the nitrogen ice depleted, the aft end was brought quickly into equilibrium with the rest of the dewar, and thus experienced the highest warmup rate.

Smooth interpolation of the low-temperature warming curve to temperatures above  $\sim 120$  K - the range measured with the FPA sensors - requires that a rate increase took place between Jan. 8 and 9. The most likely explanation for this rate increase stems from the fact that the coldwell of the NICMOS dewar houses a charcoal getter, the intention of which was to adsorb any gas that might have permeated the vacuum seals during the pre-launch cold period. The adsorption capacity of the getter is a strong function of temperature (and pressure), and as the NICMOS dewar warmed up, the getter is expected to have released nitrogen and oxygen, such that the pressure inside the coldwell rises by about 4 orders of magnitude between 70 and 120 K (Miller 1999). This could quite likely explain the second rate increase. Once all the gas is released from the getter, as much as 2.1 mg of gas could be present inside the vacuum shell of the dewar. This amount adds to the parasitic heatload for NCS to overcome. Moreover, since the amount of gas inside the coldwell varies with temperature in a self-enforcing way (higher temperature  $\rightarrow$  more gas  $\rightarrow$  increased heatload  $\rightarrow$  higher temperature), the temperature stability of the NICMOS detectors could potentially be compromised. This issue requires additional investigation.

---

1. Earlier analysis of the temperature data seemed to indicate a sudden “jump” in the warmup rates on Jan 7. This jump, which at some point was thought to be caused by a strengthening of the thermal short, could be entirely attributed to an erroneous sensor calibration above temperatures of 74 K.

**Figure 2:** Warm-up rates of cameras1 and 3, cldwell, and ctaft sensors



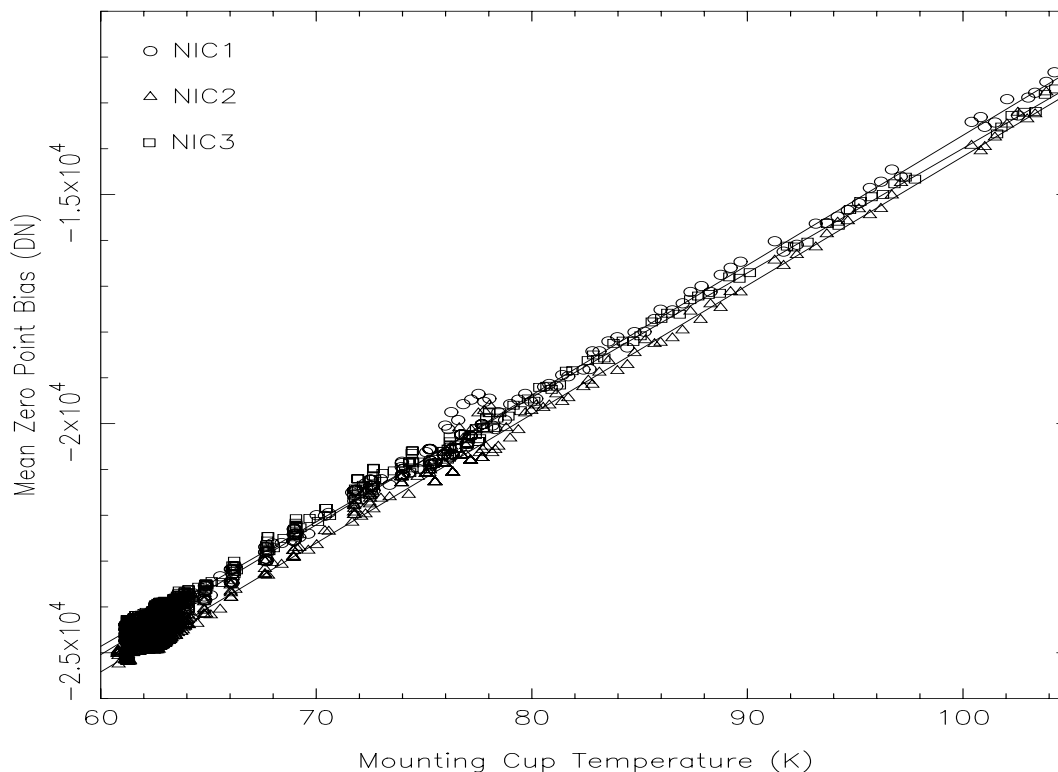
### 3. Results of the monitoring program

#### a) Bias Levels

Throughout the warm-up, the bias levels were monitored to prevent the signal in the high-responsivity pixels from reaching the maximum of the dynamic range of the A/D converters. A procedure was put in place to quickly adjust the bias offsets, in case a significant fraction (5%) of pixels in the flat field data reached the A/D limit of 32,000 counts. As Fig. 3 shows, the bias level (i.e. the mean signal in the 0th read) for all detectors changed at a rate of  $\sim 280$  counts/K, for a total change of  $\sim 15000$  counts between 62 K and 118 K. This change did not necessitate any bias adjustments during the warm-up. However, for NCS operations, the bias level should be adjusted to re-optimize the dynamic range of the detectors.

Pre-launch ground testing has shown the accurate linear relationship between bias level and detector temperature to hold to at least 120 K. Thus, one can use the bias level as a thermometer to determine the detector temperature in the range where no direct readings of the mounting cup sensors are available. This is in fact how the dark current measurements described in the next section were assigned to temperatures above 78 K.

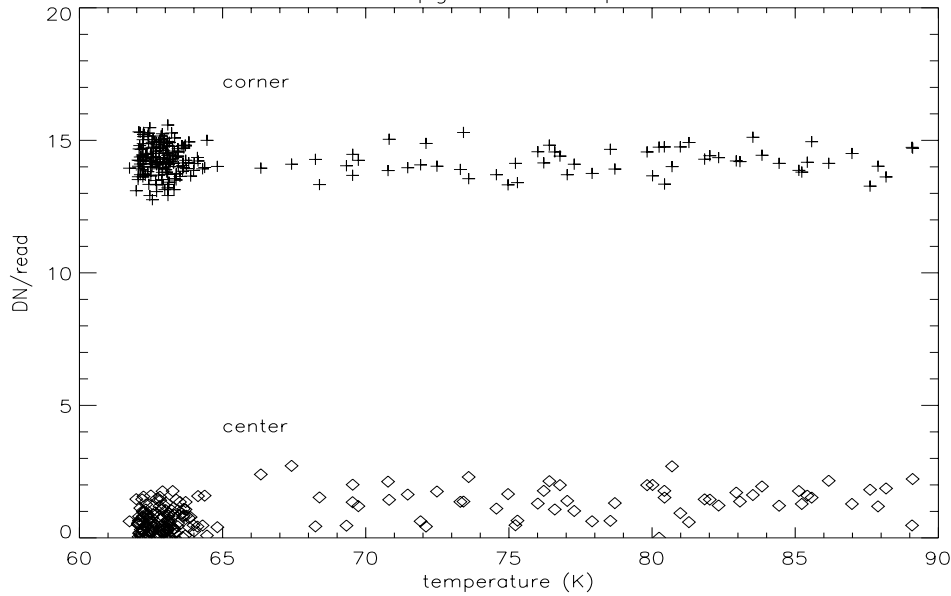
**Figure 3:** Temperature dependence of the detector bias levels



### ***b) Amplifier Glow***

The amplifier glow can be monitored by subtracting the first two read-outs in a STEP64 sequence which are only 0.3 s apart. The subtraction eliminates any contribution from the shading profile (see next section), and the short integration time does not allow a significant signal from the linear dark current. As Fig. 4 shows, the amplifier glow is constant up to a temperature of about 90 K, with typical values of  $\sim 2$  DN/read in the center of the array, and  $\sim 20$  DN/read in the corners. Thus the impact of amplifier glow on NICMOS sensitivity will be no different under NCS operation than during cycle 7.

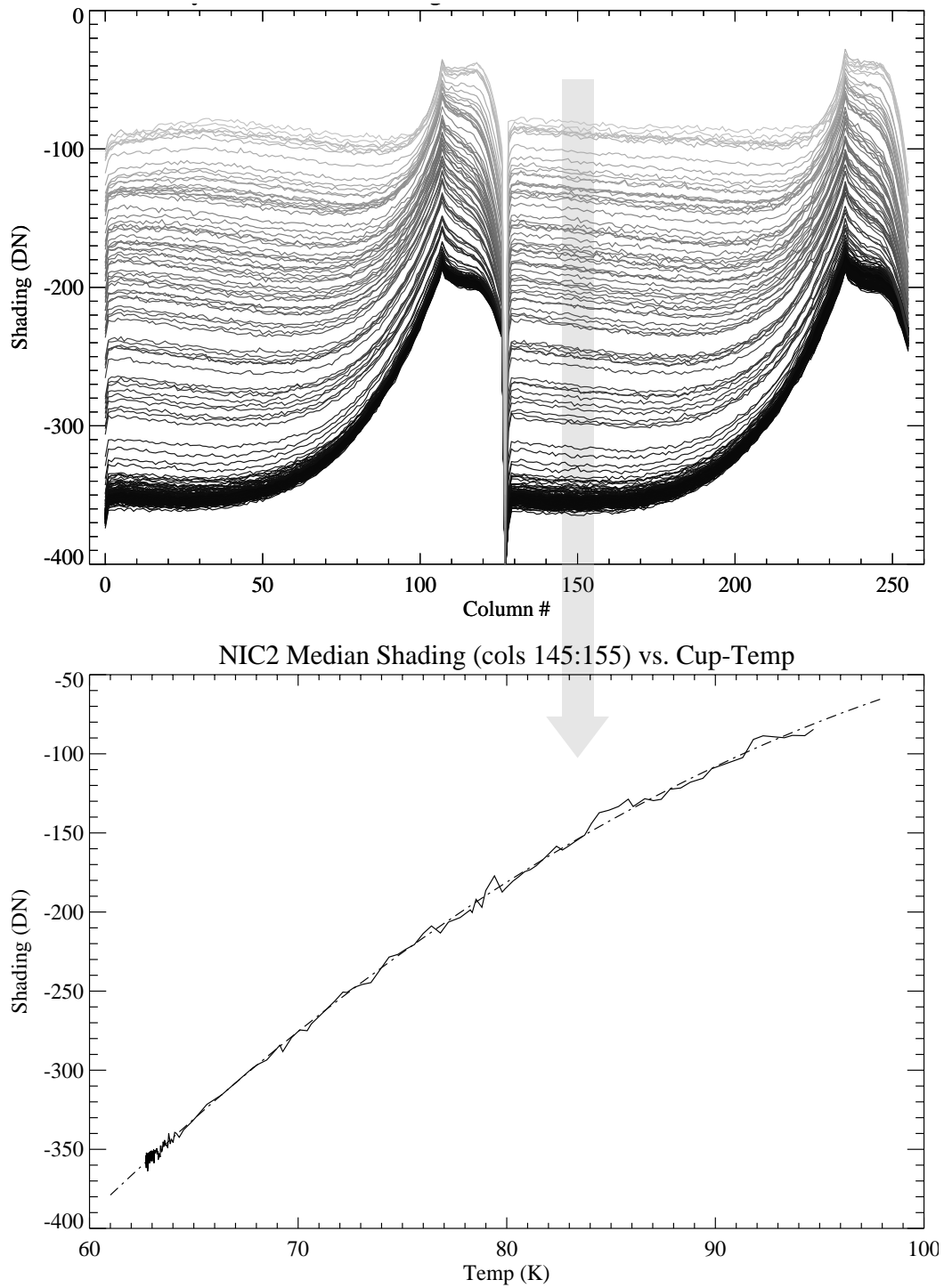
**Figure 4:** Amplifier glow signal as a function of detector temperature



### ***c) Shading profile***

The shading profile is caused by bias variations of the read-out amplifiers. It has been found to be well-correlated with the time interval between readouts ( $\Delta$ -time), over the full temperature range of the warm-up. Fig 5 (top) shows the variations of the shading profile in camera 2 with temperature throughout the warmup. The mean shading signal in columns 145 to 155 is plotted in Fig. 5 (bottom) as a function of detector temperature. It can be well modeled by a second order polynomial (dash-dotted line), a fact which can potentially be used to remove the shading during pipeline calibration (Bergeron et al. 1999). Since it is a noiseless contribution to the image, it can be completely removed by subtracting two reads with identical  $\Delta$ -times. Subtracting the first 64 s  $\Delta$ -time read from the last (after removing the accumulated amplifier glow, as described in section 3b) therefore leaves only the signal component which is linearly accumulated during the  $\sim 1000$  s time interval between those two reads. This component, which is discussed in the next paragraph, is usually referred to as the “true” or “linear” dark current in NICMOS data.

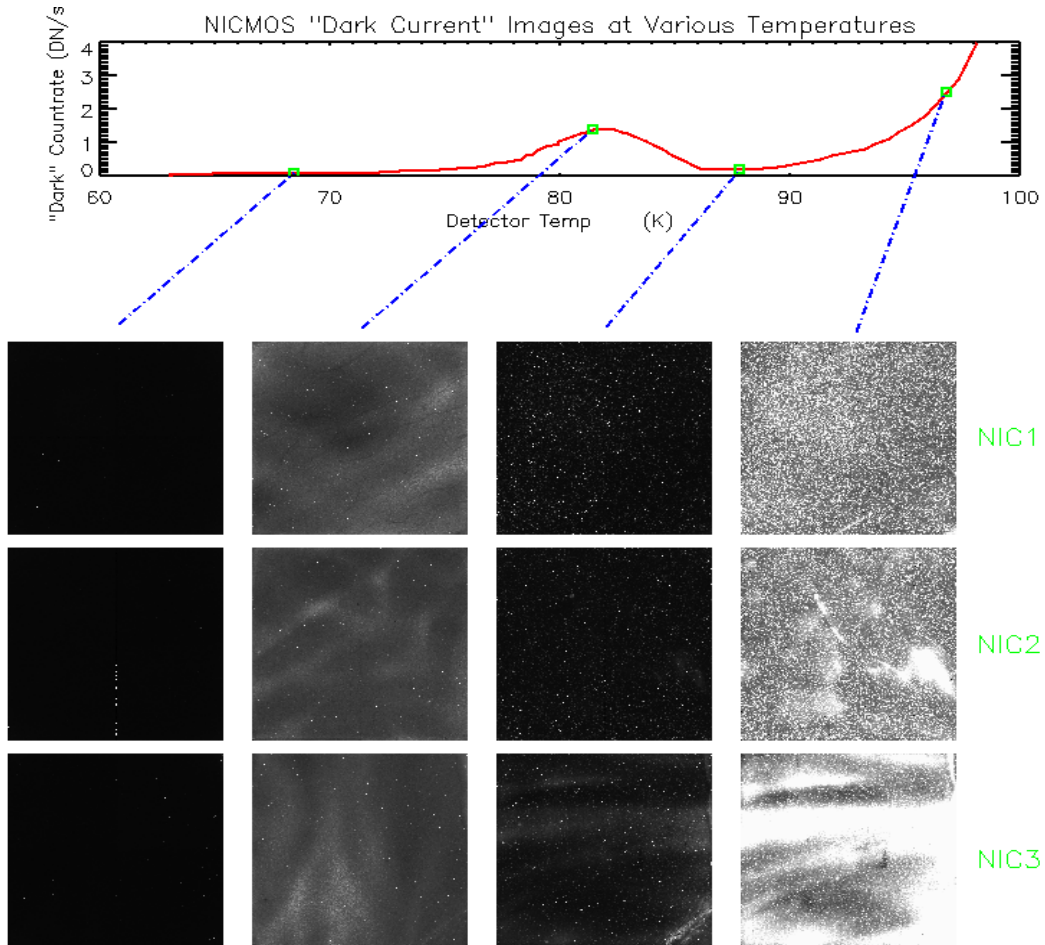
**Figure 5:** Top: temperature dependence of the shading profile in camera 2. Shown are cuts along the line direction for all dark exposures throughout the warm-up, with the lowest curves corresponding to the lowest temperatures. Bottom: mean shading signal over columns 145 to 155 (indicated by the grey arrow) as a function of detector temperature.:



*d) Linear Dark Current*

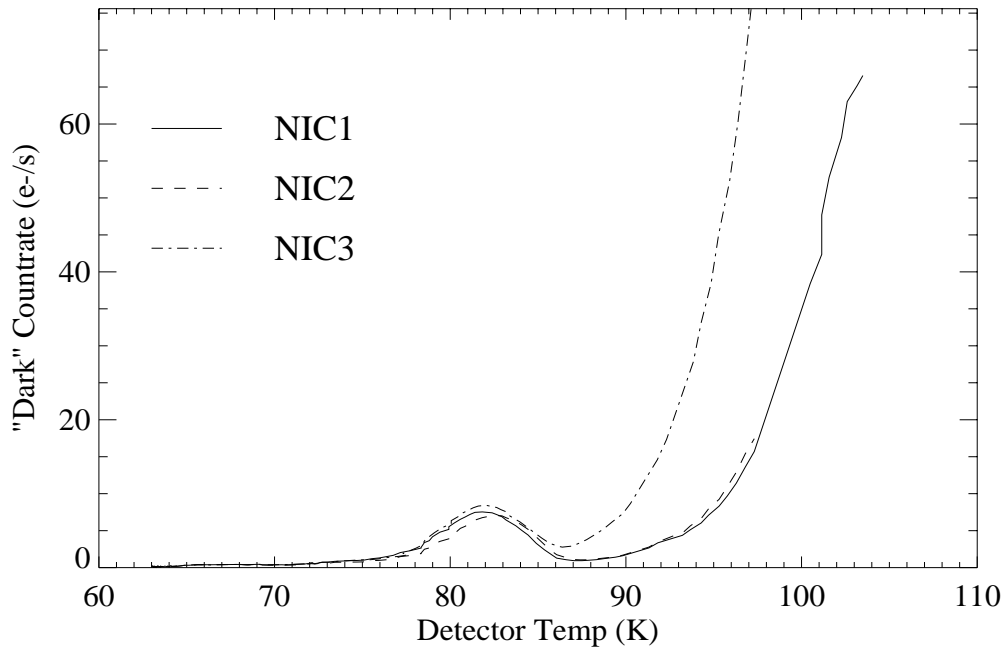
The linear dark current is measured after subtraction of amplifier glow and correction for shading. Special care was taken to minimize the impact of those measurements that were affected by passage through the South-Atlantic Anomaly (SAA). Figure 6 shows some example exposures that demonstrate the varying structure of the dark current throughout the warmup. All images are shown with an identical color stretch.

**Figure 6:** "Snapshot" dark exposures of all three cameras at temperatures of 68, 82, 88 and 97 K. Note the flatfield morphology in all cameras at 82 K..



The mean signal of all three NICMOS chips for the whole temperature range of the warm-up is plotted in Fig. 7. The characteristic increase and subsequent decline of the dark current between 80 and 95 K is an unexpected feature to which we refer as the “bump” for the remainder of this report. Since the signal responsible for the bump clearly shows the flatfield structure (Fig. 6, cmp. to Fig. 10), there is reason to believe that the bump is not due to an increased “true” dark current, but rather to a radiant signal falling onto the photosensitive layer of the detectors. Moreover, the fact that the small specks of

**Figure 7:** Median dark current signal vs. temperature for all three NICMOS cameras. The bump between 80 and 95 K is as of yet unexplained.

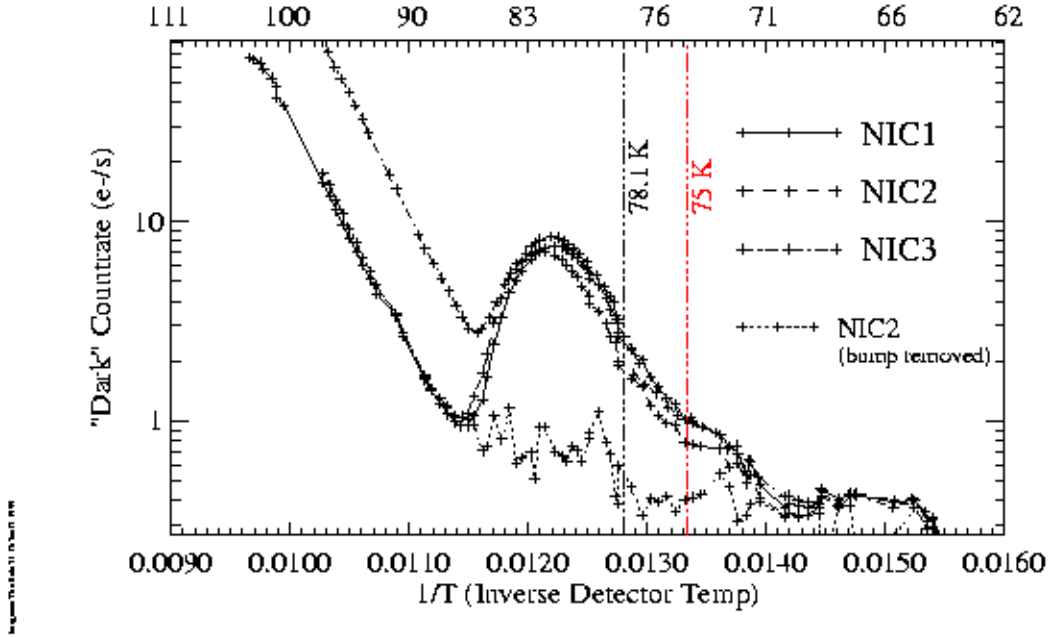


black paint known as “grot” are not visible in these images suggests that the radiation is coming from behind or within the detectors.

The idea of an additional radiant component to the dark current signal is supported by the fact that subtracting a scaled flatfield exposure - constructed from the set of CALNICA flats and weighted by the DQE curve appropriate for the respective temperature - effectively flattens the dark current image, and smoothly interpolates the dark measurements before and after the bump (lowest line in Fig. 8). This suggests that the bump is indeed due to an additional signal component whose nature is as of yet unexplained. A possible explanation for the radiant signal, which is currently being discussed, is the release of energy stored in the detector material by cosmic rays hits, by mechanisms comparable to the annealing process known from CCD chips. Additional laboratory tests are required to further investigate this theory.

The theoretical expectation for the dark current at temperatures above  $\sim 140$  K is to follow the charge carrier concentration (Cooper et al. 1993), which, in turn, rises with temperature according to the Boltzmann factor  $e^{-E/kT}$ . At temperatures between 90 and 140 K, a generation-recombination model described by Rogalski & Pietrowski (1988) provides the best agreement with the laboratory measurements of Cooper et al. (1993). The two regimes both produce a basically linear relation of  $\log(\text{dark current})$  vs  $1/T$  (Fig. 8), but with different slopes. At temperatures below 90 K, poorly understood tunneling effects are known to cause a deviation from the generation-recombination model. These result in a flattening of the dark current decrease towards colder temperatures, until a basically constant dark current is reached.

**Figure 8:** Same as Fig.7, but plotted on a logarithmic scale versus  $1/T$ . The dotted line shows the expected dark current in the case of a non-recurring bump

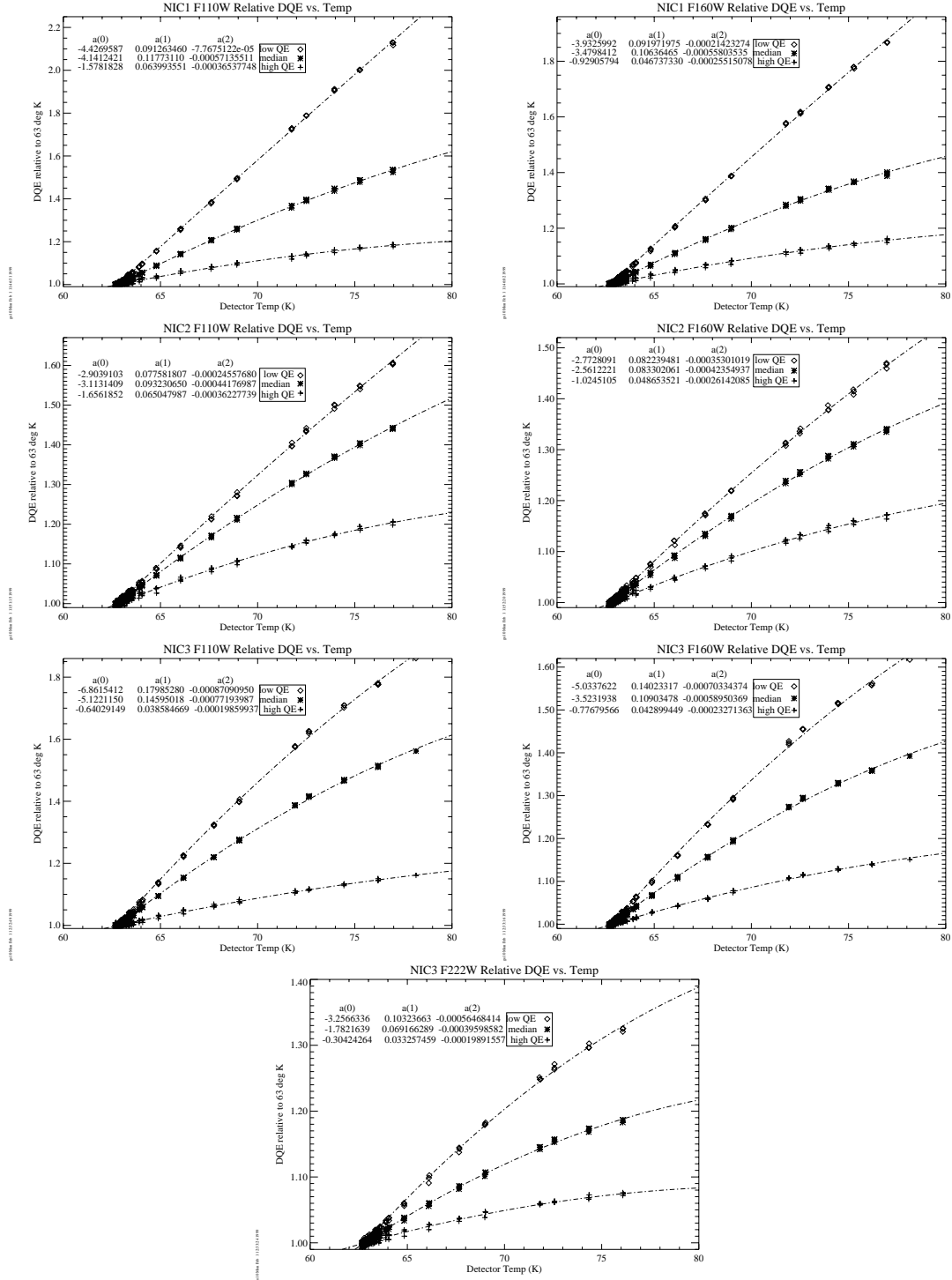


### f) Detective Quantum Efficiency

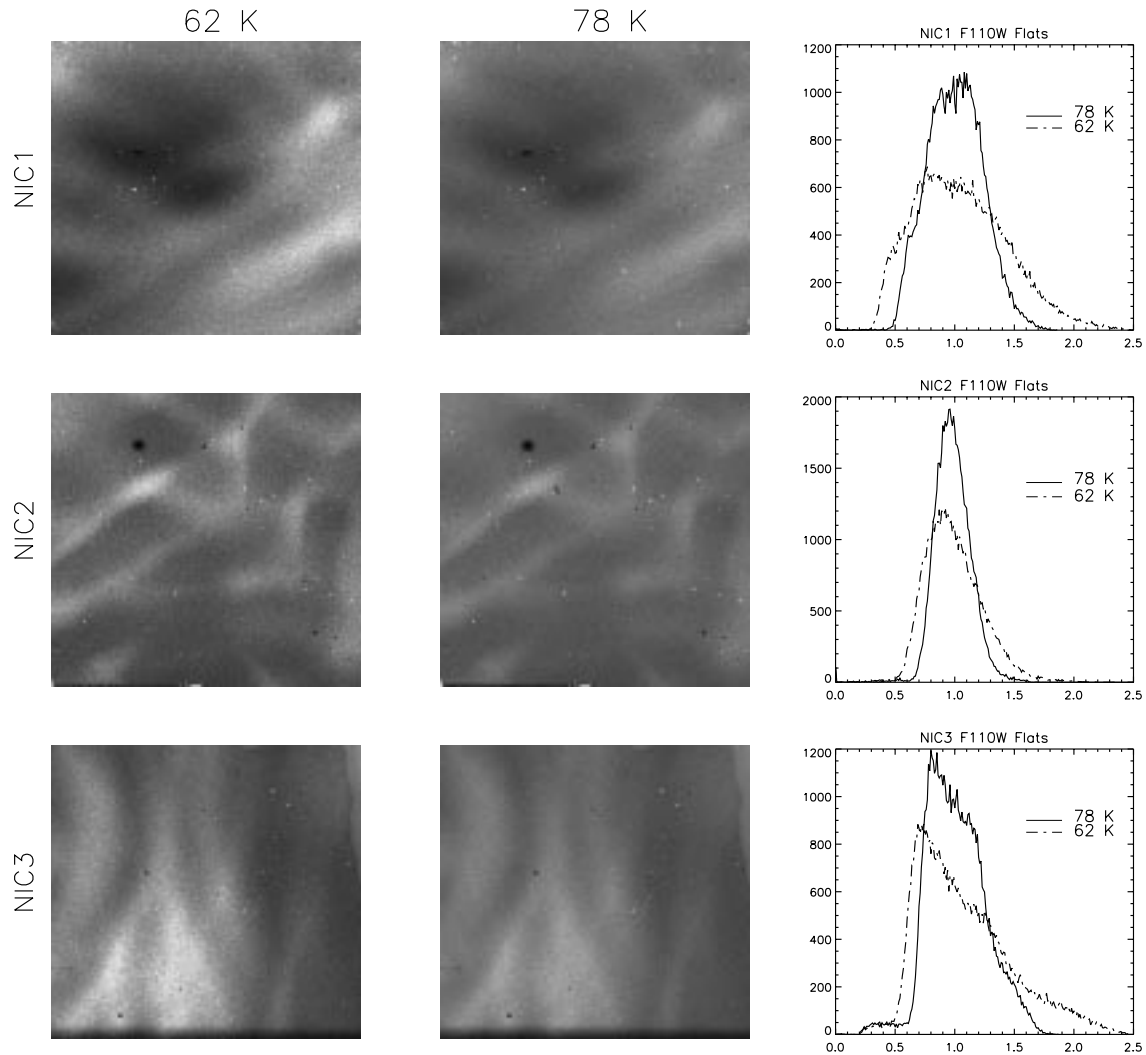
The detective quantum efficiency (DQE) is a function of temperature. The flat monitoring program was designed to determine what exactly the DQE of the NICMOS detectors at the NCS operating temperatures will be. Expectations were that low sensitivity pixels would experience a significant increase in DQE, especially at shorter wavelengths. For the analysis, we used the data as processed by the CALNICA pipeline (“\_cal” files). To first order, this should eliminate any effects caused by saturation, cosmic rays, and non-linearity. The temperature-dependent dark current and possible sky signal do not affect the analysis because each dataset consists of a pair of “lamp off” and “lamp on” exposures. Both are exposures of the (random) sky through a particular filter, but one has the additional signal from the flatfield calibration lamp located at the Field Offset Mirror (FOM). Differencing these two exposures then leaves the true flat-field response from which the DQE increase relative to pre-warmup can be derived. An additional complication is the fact that the pixel saturation levels also vary with temperature, as discussed in section 3h). All pixels that showed signs of saturation during the MULTIACCUM sequence were excluded from the analysis.

Fig. 9 shows the pixel response of all camera/filter combinations that were used during the monitoring. The three curves in each plot are a second order polynomial fit to the median DQE of the whole array and two smaller regions on the chip, which are characteristic for pixels that showed higher and lower than average sensitivities during the cryogen lifetime. The coefficients of the best fit to the data are also given in each panel.

**Figure 9:** DQE variations with temperature for all camera/filter combinations of the monitoring program. The coefficients of a second order polynomial fit are listed on the top left of each plot. For each dataset, the three curves depict a low sensitivity region on the chip (highest curve), the median DQE over the full chip (middle curve), and a high sensitivity region (bottom curve). Note that the DQE increase is highest at the shortest wavelengths.



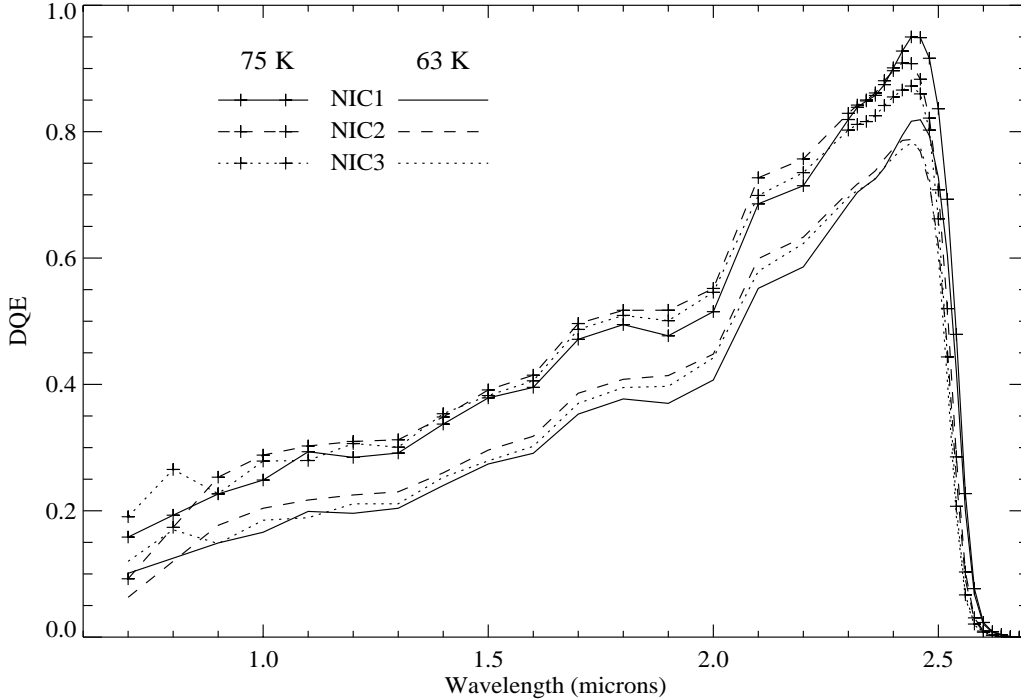
**Figure 10:** Normalized flat field exposures of all NICMOS detectors, taken through the F110W filter at temperatures of 62 K (left) and 78 K (right). The color stretch is the same for both temperatures in each camera. The histograms on the right show the “flattening” of the arrays at the higher temperature which can also be seen by comparing the images.



For all regions, the DQE increases roughly linearly between 63 K and 78 K, with a usually small curvature term. In all cameras, the linear slope is higher than average for the low-sensitivity regions, and lower than average for the high sensitivity regions. This behavior effectively flattens out the DQE variations across the array, as can be seen in Fig. 10 which compares flat field exposures of all cameras through the F110W filter at 62 and 78 K. The histograms on the right hand side in Fig. 10 clearly show a smaller spread in pixel values at the higher temperature. The average responsivity at 75 K increased by about 45% at J, 33% at H-, and 17% at K. The resulting wavelength dependence of the expected DQE for NICMOS operations at 75 K is shown in Fig. 11. Here, we have scaled the pre-

launch DQE curve, which was derived from ground testing of the detectors, to reflect the changes measured at the wavelength used in the monitoring program.

**Figure 11:** Expected NICMOS DQE as a function of wavelength for operations at 75 K (dashed line), compared to pre-launch measurements (solid line).



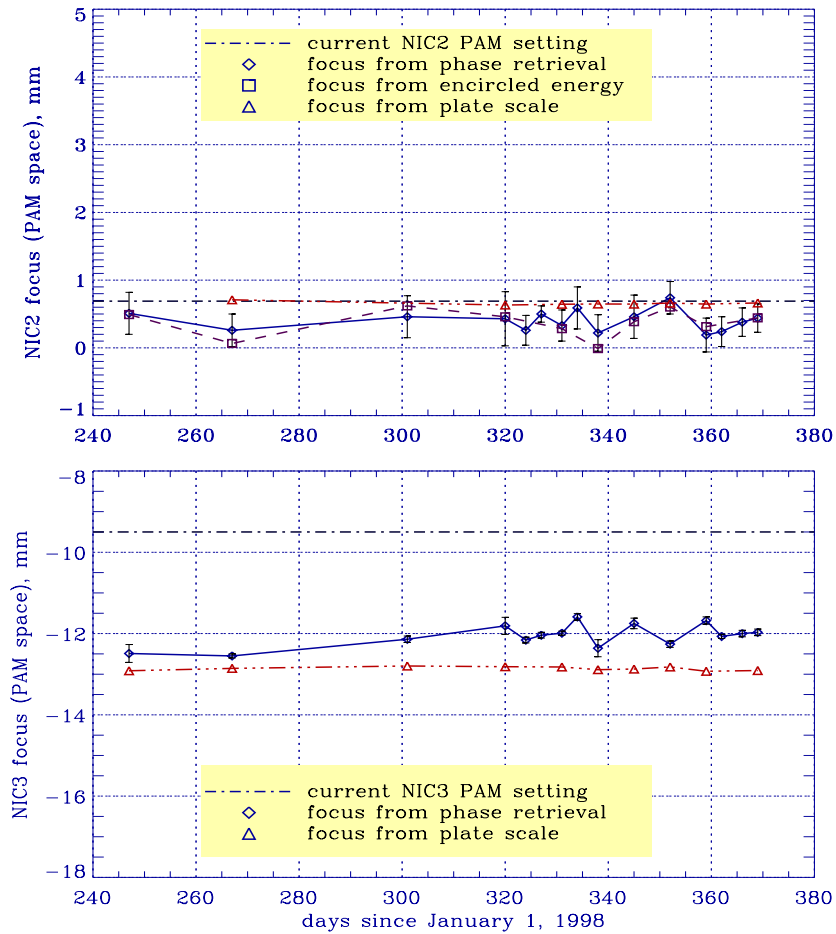
### ***g) Focus Behavior***

Fig. 12 shows the result of the focus monitoring program during the warm-up, expressed in terms of the position of the Pupil Alignment Mechanism (PAM). The best focus was determined from observations of a globular cluster by means of plate scale measurements, encircled energy calculations, as well as phase retrieval algorithms, as described in Suchkov, Bergeron, & Galas (1998). No significant variation with temperature was observed. In particular, Camera 3 remains slightly out the PAM range<sup>2</sup>. It should be noted, however, that the last dataset of the focus monitoring program was taken on Jan. 5, only two days into the warm-up, when the temperature was  $\sim 67\text{K}$ , slightly below the expected range under NCS.

---

2. However, the degradation in core energy (energy inside the first Airy ring) at the optimum accessible PAM position (-9.5 mm) is only between 13% and 27%, depending on the wavelength, without affecting the shape of the PSF (Storrs & Bergeron 1997)

**Figure 12:** Focus history of NIC2 (top) and NIC3 (bottom) throughout the warm-up.



### *h) Saturation Levels*

The capacitance of each detector pixel - which defines the saturation level - is expected to be a function of temperature. To give a visual impression of the typical behavior, Figure 13 shows the average linearity curves (count rate vs. counts) of a set of 201 pixels of the NIC2 chip that saturated<sup>3</sup> during the flatfield monitoring. Each curve represents the linearity function at a particular temperature during the warmup, with the lowest curves being taken at the lowest temperatures. As the temperature - and thus the DQE - of each pixel rises, the count rates increase, while the saturation levels decrease. There are two important conclusions that can be taken from Figure 13:

1) Since all curves are more or less parallel before saturation occurs, it is evident that the electronic gain - the conversion between photoelectrons and DN - is not a strong func-

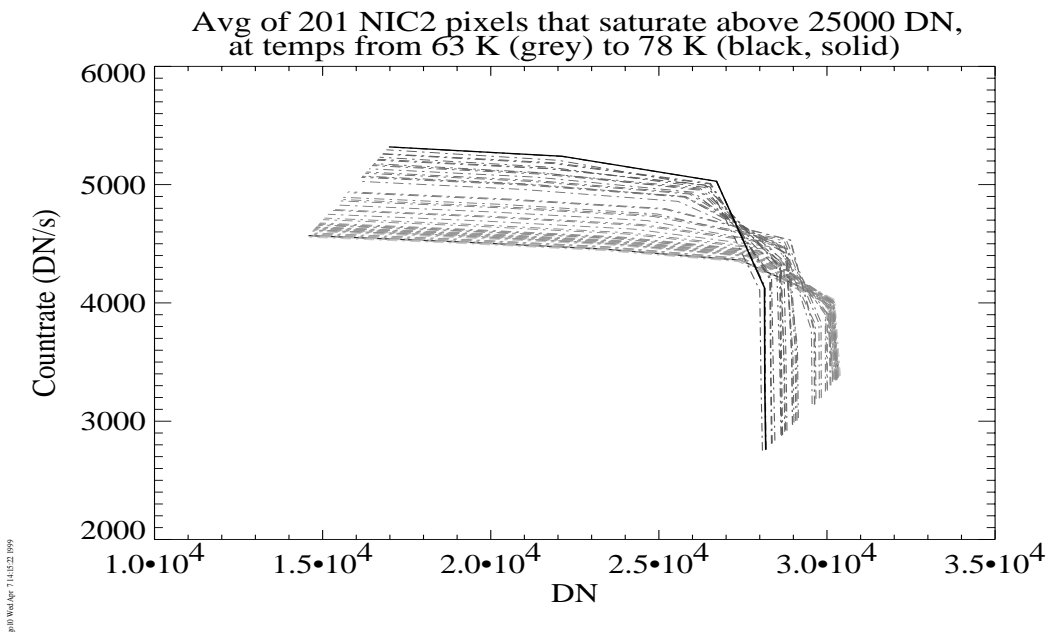
---

3. It was not intended to saturate any pixels throughout the flatfield monitoring, which is why only few pixels are available for this analysis. Saturation was defined as having a signal increase between readouts of less than 300 DN at a total of at least 25000 DN

tion of temperature. This, in turn, means that the DQE estimates of section 3f) are in fact reliable, because they are unaffected by gain changes.

2) The average pixel capacitance, which defines the saturation level, i.e. the turnover point of the linearity curve, depends on temperature. At higher temperatures, the pixels saturate earlier, as summarized in Figure 14. This means that at the NCS operating temperatures around 75 K, the dynamic range of the NICMOS detectors is reduced by ~ 15%. In order to recover the full pixel capacitance, the bias voltage can be increased slightly. However, this can potentially cause a higher dark current. Further analysis and calibration is needed to clarify this issue.

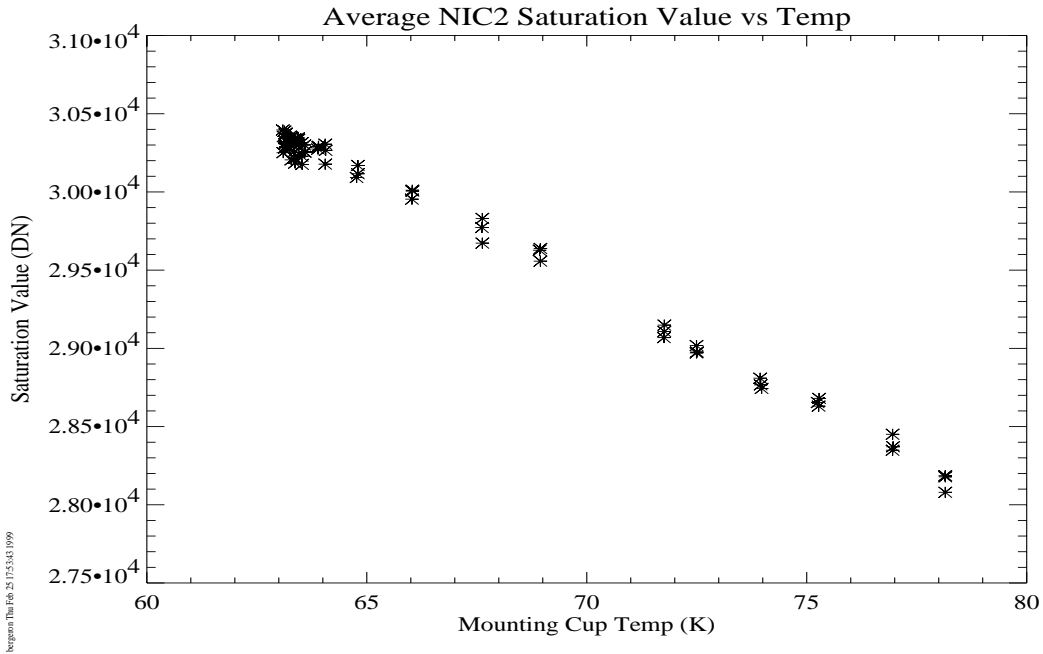
**Figure 13:** Dependence of pixel linearity curves on temperature for NIC 2. Shown are the average linearity curves of 201 saturated pixels throughout the warmup, with the lowest curves corresponding to the lowest temperatures



### *i) Detector Cosmetics*

Throughout the warm-up, no evidence was found for any significant changes in the detector cosmetics, i.e. the number of hot/dead pixels remained constant, the position and amount of “grot” did not change, and no debonding or other mechanical pixel defects were observed. The increasing number of pixels with high dark current that are responsible for the “salt and pepper” appearance of the dark current images in Fig. 6 is not yet understood, but might be attributed to the detectors not being in thermal equilibrium.

**Figure 14:** Mean saturation level vs. temperature



#### 4. Implications for NICMOS science

For a conservative estimate of NICMOS performance under NCS, we assume that the linear dark current follows the curve of Fig. 7. Under such a scenario, the average NICMOS dark current would be  $2.7 \text{ e}^-/\text{s}$  at a detector temperature of 77 K - a worst case scenario - and  $0.6 \text{ e}^-/\text{s}$  at the NCS design goal of 72.5 K. These numbers have to be viewed in relation to the other two components that contribute to the intrinsic noise in a NICMOS readout, amplifier glow and readout noise. As shown in Fig. 4, the amplifier glow is  $\sim 100 \text{ e}^-/\text{readout}$  in the corners of the array, and  $\sim 10 \text{ e}^-/\text{readout}$  in the array center, independent of temperature in the range expected for cycle 9. Therefore, the linear dark current equals the amplifier glow in the center of the array after  $\sim 4 \text{ s}$ . For  $\Delta$ -times longer than  $\sim 40 \text{ s}$ , the linear dark current will dominate amplifier glow across the whole array.

The typical single-readout<sup>4</sup> noise of the NICMOS arrays is  $\sim 30 \text{ e}^-$ . It is a non-accumulating noise contribution, equivalent to a signal of  $900 \text{ e}^-$  between readouts. Thus, for integration times longer than  $\sim 330 \text{ s}$ , the linear dark current will be the dominant noise source in NICMOS data. This will degrade the NICMOS capabilities to observe faint sources. In addition, the elevated dark current will prevent NICMOS from reaching background limited performance (BLP) in J and H, since typical sky background levels in the broad band filters (F110W and F160W, resp.) are  $0.55 \text{ e}^-/\text{s}$ , about five times less than the dark current at 77 K and about the same at 72.5 K. At longer wavelengths (K-band), the

4. The read-out noise can, in principle, be reduced by using multiple reads. However, due to the increase in amplifier glow, using multiple readouts does not reduce the readout noise by the expected factor  $\sqrt{\text{NSAMP}}$ , but can - in the best case - only reduce the level to about  $25 \text{ e}^-$

sky background is much higher due to the thermal emission from the telescope itself ( $\sim 60$   $e^-/s$ ), so BLP will still be reachable.

To assess the scientific impact of these numbers, it is important to note that the NCS specifications (GSFC STE-55, Baseline Issue, April 17, 1998) actually allow a range of temperatures for the NICMOS detectors. While the design **goal** is 72.5 K for the mounting cup sensors, the **requirements** allow mounting cup temperatures between 58 and 77 K. This wide range results in considerable uncertainty about the final NICMOS sensitivity during cycle 9.

As an example, consider a 2000 s exposure of a deep field. For simplicity, we assume that the total integration time of 2000 s is taken in ACCUM mode, with no intermediate reads. In that case, we can neglect the amplifier glow as a noise source, since its contribution to the total noise is much smaller than the read noise. Before the warm-up, the total noise in the image would have been  $\sqrt{900 + 2000 \cdot 0.1 e^-} = 33 e^-$ . The worst case dark current at 77 K of  $2.7 e^-$  would raise the noise level to  $\sim 79 e^-$ , about 2.4 times higher.

Since the DQE at the higher temperature is typically 40% higher, the effective signal-to-noise ratio in cycle 9 will be reduced to 58%, or 0.6 magnitudes, compared to cycle 7. However, at the NCS design goal of 72.5 K, the expected noise is only  $46 e^-$ , and with the higher DQE, the resulting signal-to noise ratio is basically identical to that achieved during cycle 7. In other words, with NCS working according to its design goals, the **NICMOS science capabilities will be fully restored for cycle 9**, even with worst case assumptions about the dark current.

If, on the other hand, the bump is the result of a non-recurring radiant signal, the dark current over most of the NCS temperature range will be  $\sim 0.4 e^-/s$  (lowest curve in Fig. 7), resulting in a total noise of  $\sim 41 e^-/s$ . In this case, the increased DQE will outweigh the higher dark current, and therefore slightly improve the scientific performance for cycle 9, **independent of the actual operating temperature**.

## 5. Conclusions and Recommendations

From the above example, it is clear that the operating temperature for NICMOS under NCS is the most important parameter for an estimate of the scientific performance, since both DQE and dark current are strongly dependent on temperature in the range in question. Another direct consequence is that the stability of the operating temperature is crucial for the complexity of NICMOS calibration for cycle 9. In this regard, the outgassing of the charcoal getter discussed in section 2 is a potential problem that requires a more detailed analysis.

In anticipation of eventual temperature variations during normal NICMOS operations, all or parts of the monitoring program should be repeated during the initial NCS cooldown after SM3 in order to obtain up-to-date curves of DQE and dark current vs. temperature

for as many filters as possible. This could allow operation at different detector temperatures without the need for a calibration program every time the NCS was unable to maintain stability or a setpoint was altered.

To summarize, if the NCS meets the design goals, and under the assumption of a repeatable dark current behavior, NICMOS will reach the same sensitivity as during cycle 7, and will continue to provide a powerful and unique tool to the astronomical community.

We are grateful to D. Calzetti for the planning and implementation of the monitoring program. We also wish to thank A. Nota, R. Doxsey, and M. Hauser for valuable comments on earlier versions of this ISR.

## **6. References**

- Bergeron, L. E. 1999, Instr. Sc. Rep. NICMOS-99-???, in prep.
- Cooper, D. E. et al. 1993, Proc. of SPIE 1946, 170
- Miller, C. D. 1998, Ball Aerospace Syst. Eng. Rep. 30217-CRYO-004
- Rogalski, A. & Pietrowski, J. 1988, "Progr. in Quantum Electr.", Vol. 12, no. 2/3, 87
- Storrs, A. & Bergeron, L.E. 1997, Instr. Sc. Rep. NICMOS-97-027
- Suchkov, A., Bergeron, E. L., & Galas, G. 1998, Instr. Sc. Rep. NICMOS-98-004